Tracking Electrons and Atoms in a Photoexcited Metalloporphyrin by X-ray Transient Absorption Spectroscopy

ARTICLE *in* JOURNAL OF THE AMERICAN CHEMICAL SOCIETY · SEPTEMBER 2007

Impact Factor: 12.11 · DOI: 10.1021/ja072979v · Source: PubMed

J|A|C|S
COMMUNICATIONS

Published on Web 07/18/2007

Tracking Electrons and Atoms in a Photoexcited Metalloporphyrin by X-ray Transient Absorption Spectroscopy

Lin X. Chen,*,† Xiaoyi Zhang,†,‡ Erik C. Wasinger,† Klaus Attenkofer,‡ Guy Jennings,‡ Ana Z. Muresan,§ and Jonathan S. Lindsey§

Chemistry Division and X-ray Science Division, Argonne National Laboratory, Argonne, Illinois 60439, and Department of Chemistry, North Carolina State University, Raleigh, North Carolina 27695

Received May 3, 2007; E-mail: lchen@anl.gov

Metalloporphyrins are versatile substrates in various light-driven chemical reactions, enabling intra- and intermolecular energy/electron redistribution that triggers chemical processes.[1−3] Details concerning the electronic configuration and molecular geometry of excited-state metalloporphyrins and their influence on light-activated functions have mainly eluded direct experimentation. Although excited-state dynamics for photoinduced electron and energy transfer have been measured by ultrafast laser spectroscopy for various metalloporphyrin systems,[4−9] structural factors that account for the variation of excited-state kinetics are often unclear. In particular, electronic configurations and coordination geometry of the central metal ion in the excited states, such as electron occupation and molecular orbital (MO) energy levels, often remain vague because metal-centered electronic states are sometimes optically "dark" or their optical signatures are masked by other stronger features, making it difficult to track the location of the transition metal d electrons in the excited states. Thus, theoretical calculations very often are the predominant if not sole means of obtaining MO energy levels and electronic configurations of excited-state metalloporphyrins.[10−12]

Rapid progress has been made in recent years in resolving transient molecular structures in solution (where most chemical reactions take place) using laser-initiated time-resolved X-ray absorption spectroscopy[13−17] which is referred to as X-ray transient absorption spectroscopy (XTA) in this study. Here we present simultaneous tracking of the electronic and molecular configurations for an excited state of nickeltetramesitylporphyrin (NiTMP), in a dilute toluene solution (1.5 mM) with a 200 ps lifetime using XTA. NiTMP has been chosen because it represents metalloporphyrins with open-shell transition metals whose excited states are short-lived and poorly understood due to the coupling between the MOs involved in the initial (π, π*) excited state with metal d electron-dominant MOs involved in light-activated redox reactions.

The proposed excited-state pathway of NiTMP in noncoordinating solvents is outlined in Figure 1A, on the basis of previous studies of NiTPP (nickeltetraphenylporphyrin),[4] an analogous molecule. The kinetics parameters of NiTMP were obtained by our own optical transient absorption measurements. The electronic configuration of Ni(II) ($3d^8$) in a nearly square-planar ground state S_0 has an empty $3d_{x^2-y^2}$ MO and a doubly occupied $3d_{z^2}$ MO according to ligand field theory.[18] The $S_0 \rightarrow S_{1,2}$ transitions in NiTMP can be induced by exciting the B- (or Soret) band. Within 350 fs following the excitation, the S_1 or S_2 (π, π*) state is believed to convert, through energy transfer followed by intersystem crossing, to an intermediate state T_1' that then undergoes vibrational relaxation in less than 20 ps to a relaxed triplet state, T_1, with a presumed

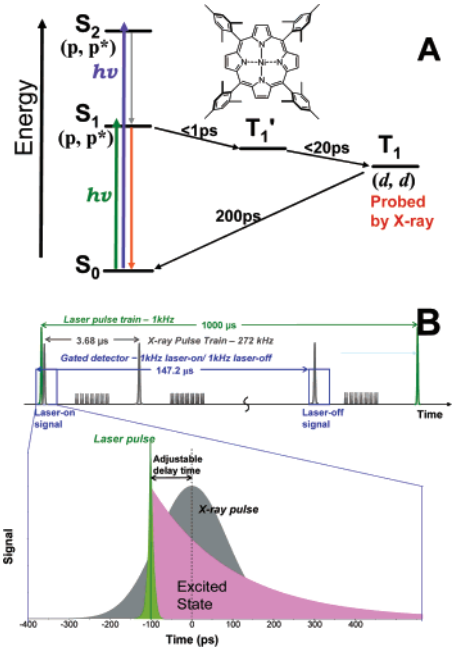

Figure 1. (A) Photoexcitation pathways of NiTMP in toluene solution according to previous work on NiTPP.[4] (B) The timing scheme of the XTA experiments carried out at Beamline 11ID-D, the Advanced Photon Source of Argonne National Laboratory. Please see the Supporting Information for more details. The X-ray probe pulses were extracted from a train of electron bunches under a hybrid timing mode operation as shown. Output signals from a solid-state germanium detector array were electronically gated with two sets of gate signals, one of which coincided with the laser pulses for the laser-on spectrum, and the other of which was at 40 round trips of X-ray pulses later for the laser-off spectrum. The delay time between the laser and the X-ray pulses as shown is 100 ps.

$^3(3d_{x^2-y^2}, 3d_{z^2})$ configuration, where $3d_{x^2-y^2}$ and $3d_{z^2}$ MOs are each singly occupied.[4,19−21] Finally, the T_1 state returns to the S_0 state in approximately 200 ps. The electronic configurations of these excited states have been assigned largely according to computational results that describe charge-transfer states of transition metalloporphyrins with unfilled d orbitals. The geometric structures of these excited states, although inferred by resonance Raman spectroscopy[22−24] and calculated by theoretical methods,[11,12] are still subject to many uncertainties. Moreover, the electronic configuration of the T_1' state is not entirely clear. Therefore, it is desirable to simultaneously track electronic and molecular configurations for these excited states in order to understand the correlations between electronic and molecular structural factors with reaction kinetics and pathways.

We have extended the optical "pump−probe" transient absorption spectroscopy to the X-ray regime where a laser pulse at 527 nm is used to induce the $S_0 \rightarrow S_1$ transition and an X-ray pulse from a

† Chemistry Division, Argonne National Laboratory.
‡ X-ray Science Division, Argonne National Laboratory.
§ North Carolina State University.

10.1021/ja072979v CCC: $37.00

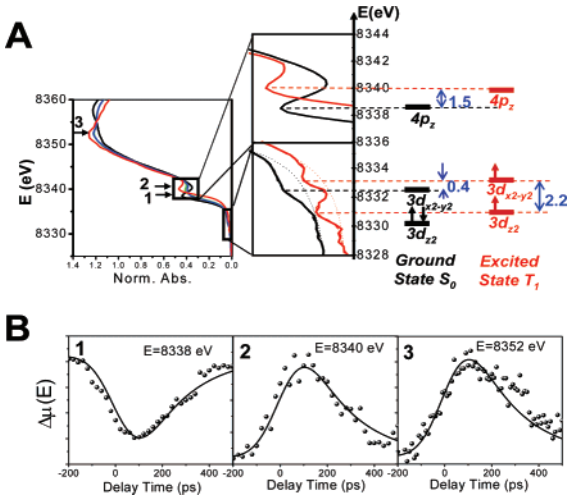

Figure 2. (A) XTA spectra in the near Ni K-edge region and their correlation with the MO energy levels of NiTMP (black, laser-off; green, laser-on at $t = 0$; blue, laser-on at $t = 100$ ps; and red, the T_1 state spectrum; t = delay time). The X-ray absorption near-edge structure (XANES) spectra of the Ni K-edge is rotated counter-clockwise by 90° from the conventional display with highlighted regions enlarged showing the pre-edge region for the 1s → 3d transitions, and the transition edge region for the 1s → $4p_z$ transitions. (B) XTA difference signals (laser-on−laser-off) as functions of the delay time between the laser and the X-ray pulses taken at three X-ray photon energies labeled by arrows in XANES spectra in (A).

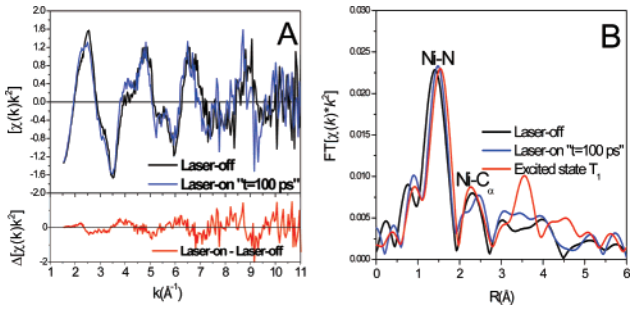

Figure 3. (A) EXAFS spectra for NiTMP with the laser-off and laser-on conditions, respectively, at the delay time of 100 ps, where the maximal spectral differences were observed between the two conditions. The difference spectrum displayed in the bottom shows systematic variations throughout the entire spectral range originated from distance changes between Ni and neighboring atoms; (B) the phase uncorrected Fourier-transformed EXAFS spectra of NiTMP, showing the porphyrin ring expansion by the simultaneous elongation of Ni−N and Ni−C_α distances shown as the peak shift to longer R in the T_1 state. The shift of the Ni−C_α distance is masked by multiscattering contributions and is uncovered by the data analysis. The distances presented by the peaks are shorter than their actual values obtained from data analysis results in Table 1, where the multiple scatterings are also included.

synchrotron source is used to probe the excited states (Figure 1B). In particular, the electronic configuration and the geometry of the T_1 state is interrogated in this study because its precursors, the S_1 and T_1' states, are too short-lived to be captured by X-ray pulses from the current synchrotron sources (approximately 160 ps fwhm). The experimental details can be found in the Supporting Information.

Figure 2A presents XTA spectra at the Ni K-edge (8333 eV) taken under different conditions: laser-off, laser-on at the delay time $t = 0$, laser-on at $t = 100$ ps, and the T_1 spectrum (extracted from the laser-on spectrum by properly subtracting the remaining ground-state contribution; see the Supporting Information). In the 1s → 3d pre-edge region, ligand field theory predicts a single transition[25] to the only unfilled Ni $3d_{x^2-y^2}$ orbital in the S_0 state, which is observed experimentally at 8332.8 eV. However, two features at 8331.0 and 8333.2 eV are observed in the T_1 state spectrum, which are consequently attributed to transitions from the Ni 1s orbital to the half-vacant predominantly $3d_{x^2-y^2}$ and $3d_{z^2}$ MOs, respectively. Hence, the pre-edge spectrum directly depicts the electronic configuration of the T_1 state as singly occupied $3d_{x^2-y^2}$ and $3d_{z^2}$, with an energy splitting of 2.2 eV between them in the final state. Such results are not easily obtainable by other techniques, including optical transient absorption spectroscopy. Moreover, an increase of 0.4 eV in the $3d_{x^2-y^2}$ MO energy in the T_1 state relative to that of the S_0 state is experimentally observed, a result obtainable heretofore only via theoretical calculations. Therefore, XTA directly measures excited-state MO energy levels through X-ray induced electronic transitions from the core to valence levels while the molecules are optically excited. This method is particularly suited for correlating molecular geometry with electronic configurations and MO energy levels when the excited state is optically dark or overwhelmed by other strongly absorbing or emitting states.

In the region of the transition edge from 8337 to 8343 eV, the spectra exhibit a distinctive feature assigned as the dipole allowed 1s → $4p_z$ transition[26] (Figure 2A). This transition is shifted to 1.5 eV higher in energy in the T_1 state than in the S_0 state. Meanwhile, changes in the "white line" peak region of 8350−8360 eV are also observed, which are attributed to energy level shifts of $4p_x$ and $4p_y$ MOs convoluted with multiple scattering contributions in EXAFS (extended X-ray absorption fine structure). An accurate analysis in this region to determine precise contributions from different sources is beyond the scope of this report.

Figure 2B displays the X-ray fluorescence difference signals $\Delta\mu(E)$ (laser-on−laser-off) as functions of the delay time between the laser and the X-ray pulses at three X-ray photon energies that characterize specific electronic transitions induced by X-rays. As a result of the laser excitation at 527 nm, the 1s → $4p_z$ transition intensity at 8338 eV for the S_0 state decreases while a new peak emerges at 8340 eV characterizing the same transition for the T_1 state, indicating the correlation between the two states. These signals are analogous to the ground-state bleaching and excited-state absorption signals in optical transient absorption spectroscopy. Although the current XTA time resolution is too low to resolve the depletion and the rise of the S_0 and T_1 states, all three time scans (Figure 2B) agree with the calculated convolution of a Gaussian function for the X-ray pulse with 160 ps fwhm and an exponential decay function for the T_1 state population with a 200 ps time constant. Hence XTA can resolve the electronic and structural dynamics, potentially their coherence as well, by selectively monitoring time evolution of specific X-ray induced electronic transitions after the laser excitation.

As the conversion of the excited NiTMP proceeds through the energy cascade along the path $S_1 \rightarrow T_1' \rightarrow T_1$, the excess energy from the (π, π^*) state generates vibrationally hot states accompanying electron redistribution,[4,21,27] resulting in molecular geometry rearrangements. These structural changes can be extracted from the EXAFS spectra in Figure 3A, where the laser-off and laser-on at $t = 100$ ps spectra are clearly different in oscillation frequency and phase. Fourier-transformed EXAFS spectra in Figure 3B show the lengthening of the average Ni−N and Ni−C_α distances (without phase corrections) in the T_1 state, determined to be 0.08 and 0.07 Å, respectively (Table 1), consistent with an expansion of the porphyrin ring. It is conceivable that the addition of one electron to the higher energy antibonding $3d_{x^2-y^2}$ MO in the T_1 state could cause stronger electrostatic repulsion and further reduce the bond order for Ni−N bonds, resulting in longer Ni−N bond distances. As the porphyrin ring expands in the T_1 state, the electron density on Ni(II) through σ bonding and π conjugation decreases while its

Table 1. Structural Parameters of the Ground- and the Excited-State NiTMP in Toluene Extracted from EXAFS Spectra (*N*, Number of the Atom Pairs, *R*, Distance, σ^2, Debye−Waller Factor, and ΔE, Energy Shift in the Fitting)[a]

state	atom pair	*N*	*R* (Å)	σ^2 (Å^2)	ΔE_0 (eV)
ground	Ni−N	4	1.90	0.001	8.8
	Ni−C_α	8	2.92	0.006	8.8
excited	Ni−N	4	1.98	0.001	8.5
	Ni−C_α	8	2.99	0.002	8.5

[a] The data analysis/fitting was carried out using the simulated solid-state NiTPP[28] XAFS spectrum as reference from FEFF8.0 program.[29,30] The distances beyond the second nearest neighbors are not listed because they require higher signal-to-noise ratio in the experimental data than those currently available. The precision for distance *R* is about 0.02 Å.

effective charge increases compared to that of the S_0 state, which may consequently cause an energy upshift of the $1s \rightarrow 3d_{x^2-y^2}$ and $1s \rightarrow 4p_z$ transitions in the T_1 state (Figure 2A).

The electronic configuration and molecular geometry for the T_1 state of NiTMP simultaneously obtained through this study reveal the following: (i) the T_1 state has a ($3d_{x^2-y^2}$, $3d_{z^2}$) electronic configuration with singly occupied $3d_{x^2-y^2}$ and $3d_{z^2}$ MOs; (ii) the energy gap between $3d_{x^2-y^2}$ and $3d_{z^2}$ in the T_1 state is approximately 2.2 eV; (iii) the primarily metal $3d_{x^2-y^2}$ and $4p_z$ MOs in the T_1 state shift by 0.4 and 1.5 eV to higher energy, respectively, than the corresponding MOs of the ground state S_0; and (iv) the porphyrin ring in the T_1 state expands driven by the electronic density shifts and excess vibrational energies following the conversion $^1(\pi, \pi^*) \rightarrow (3d_{x^2-y^2}, 3d_{z^2})$.

The above example clearly demonstrates the prospects of XTA for simultaneously tracking the electronic configurations and atomic coordinates in metal complexes along their excited-state pathways. While valence electrons of molecules are promoted to higher energy MOs by laser photons, XTA spectra can probe electronic transitions from core to valence levels induced by X-rays. This provides an alternative means for obtaining metal excited-state electronic configurations that may otherwise be inaccessible by optical transient absorption spectroscopy. These results can directly verify and guide theoretical calculations and spectroscopic assignments for excited-state metal complexes. In particular, the XTA method can selectively probe the time evolution of the electron occupation and the energy level for a particular MO (e.g., $4p_z$) after the photoexcitation, as seen in Figure 2B. This capability validates the great potential of XTA using next-generation X-ray sources, namely, X-ray free electron lasers with selected X-ray photon energies, in resolving excited-state kinetics and coherence with fs time resolution. Hence, accurate structural and kinetic information can be obtained not only for relaxed excited states but likely also for evanescent transition states (i.e., the T_1' state) or coherent atomic motions. These capabilities will make simultaneously visualizing electronic and molecular structures during photochemical reactions a reality, enabling new insight into reaction mechanisms and validating the rational design of molecules for solar energy conversion, catalysis, and molecular devices.

Acknowledgment. This work is supported by the Division of Chemical Sciences, Office of Basic Energy Sciences, U.S. Department of Energy under contracts DE-AC02-06CH11357 (L.X.C., X.Z., E.C.W., K.A., and G.J.) and DE-FG02-96ER14632 (J.S.L. and A.Z.M.). The authors would like to thank Dr. Bingxing Yang of the Advanced Photon Source for measuring temporal characteristics of X-ray pulses during the experiment. Use of the Advanced Photon Source was supported by the U.S. Department of Energy, Office of Science, Office of Basic Energy Sciences, under Contract No. DE-AC02-06CH11357.

Supporting Information Available: The timing scheme and experimental setup of the XTA at Beamline 11IDD, the Advanced Photon Source in Argonne National Laboratory and EXAFS data analyses and fitting results. This material is available free of charge via the Internet at http://pubs.acs.org.

References

(1) Gust, D.; Moore, T. A.; Moore, A. L. *Acc. Chem. Res.* **2001**, *34*, 40−48.
(2) Holten, D.; Bocian, D. F.; Lindsey, J. S. *Acc. Chem. Res.* **2002**, *35*, 57−69.
(3) Rosenthal, J.; Bachman, J.; Dempsey, J. L.; Esswein, A. J.; Gray, T. G.; Hodgkiss, J. M.; Manke, D. R.; Luckett, T. D.; Pistorio, B. J.; Veige, A. S.; Nocera, D. G. *Coord. Chem. Rev.* **2005**, *249*, 1316−1326.
(4) Rodriguez, J.; Holten, D. *J. Chem. Phys.* **1989**, *91*, 3525−3531.
(5) Kumble, R.; Palese, S.; Lin, V. S. Y.; Therien, M. J.; Hochstrasser, R. M. *J. Am. Chem. Soc.* **1998**, *120*, 11489−11498.
(6) Yang, S. I.; Lammi, R. K.; Prathapan, S.; Miller, M. A.; Seth, J.; Diers, J. R.; Bocian, D. F.; Lindsey, J. S.; Holten, D. *J. Mater. Chem.* **2001**, *11*, 2420−2430.
(7) Franzen, S.; Kiger, L.; Poyart, C.; Martin, J.-L. *Biophys. J.* **2001**, *80*, 2372−2385.
(8) Yu, H. Z.; Baskin, J. S.; Zewail, A. H. *J. Phys. Chem. A* **2002**, *106*, 9845−9854.
(9) Pettersson, K.; Kils, K.; Martensson, J.; Albinsson, B. *J. Am. Chem. Soc.* **2004**, *126*, 6710−6719.
(10) Nguyen, K. A.; Pachter, R. *J. Chem. Phys.* **2003**, *118*, 5802−5810.
(11) Patchkovskii, S.; Kozlowski, P. M.; Zgierski, M. Z. *J. Chem. Phys.* **2004**, *121*, 1317−1324.
(12) Rosa, A.; Ricciardi, G.; Baerends, E. J.; Zimin, M.; Rodgers, M. A. J.; Matsumoto, T.; Ono, N. *Inorg. Chem.* **2005**, *44*, 6609−6622.
(13) Chen, L. X.; Jager, W. J. H.; Jennings, G.; Gosztola, D. J.; Munkholm, A.; Hessler, J. P. *Science* **2001**, *292*, 262−264.
(14) Saes, M.; Bressler, C.; Abela, R.; Grolimund, D.; Johnson, S. L.; Heimann, P. A.; Chergui, M. *Phys. Rev. Lett.* **2003**, *90*, 047403/1−047403/4.
(15) Chen, L. X. *Angew. Chem., Int. Ed.* **2004**, *43*, 2886−2905.
(16) Chen, L. X. *Annu. Rev. Phys. Chem.* **2005**, *56*, 221−254.
(17) Khalil, M.; Marcus, M. A.; Smeigh, A. L.; McCusker, J. K.; Chong, H. H. W.; Schoenlein, R. W. *J. Phys. Chem. A* **2006**, *110*, 38−44.
(18) Ballhausen, C. J. *Introduction to Ligand Field Theory*; McGraw-Hill: New York, 1962.
(19) Kim, D.; Kirmaier, C.; Holten, D. *Chem. Phys.* **1983**, *75*, 305−322.
(20) Gentemann, S.; Nelson, N. Y.; Jaquinod, L.; Nurco, D. J.; Leung, S. H.; Medforth, C. J.; Smith, K. M.; Fajer, J.; Holten, D. *J. Phys. Chem. B* **1997**, *101*, 1247−1254.
(21) Eom, H. S.; Jeoung, S. C.; Kim, D.; Ha, J.-H.; Kim, Y.-R. *J. Phys. Chem. A* **1997**, *101*, 3661−3669.
(22) Jentzen, W.; Unger, E.; Karvounis, G.; Shelnutt, J. A.; Dreybrodt, W.; Schweitzer-Stenner, R. *J. Phys. Chem.* **1996**, *100*, 14184−14191.
(23) Rush, T. S., III; Kozlowski, P. M.; Piffat, C. A.; Kumble, R.; Zgierski, M. Z.; Spiro, T. G. *J. Phys. Chem. B* **2000**, *104*, 5020−5034.
(24) Huang, Q.; Medforth, C. J.; Schweitzer-Stenner, R. *J. Phys. Chem. A* **2005**, *109*, 10493−10502.
(25) Westre, T. E.; Kennepohl, P.; DeWitt, J. G.; Hedman, B.; Hodgson, K. O.; Solomon, E. I. *J. Am. Chem. Soc.* **1997**, *119*, 6297−6314.
(26) Kau, L.-S.; Spira-Solomon, D. J.; Penner-Hahn, J. E.; Hodgson, K. O.; Solomon, E. I. *J. Am. Chem. Soc.* **1987**, *109*, 6433−6442.
(27) Mizutani, Y.; Kitagawa, T. *J. Mol. Liq.* **2001**, *90*, 233−242.
(28) McLean, A. L.; Foran, G. J.; Kennedy, B. J.; Turner, P.; Hambley, T. W. *Aust. J. Chem.* **1996**, *49*, 1273−1278.
(29) Deleon, J. M.; Rehr, J. J.; Zabinsky, S. I.; Albers, R. C. *Phys. Rev. B* **1991**, *44*, 4146−4156.
(30) Rehr, J. J.; Mustre de Leon, J.; Zabinsky, S. I.; Albers, R. C. *J. Am. Chem. Soc.* **1991**, *113*, 5135−5140.

JA072979V